A 3D pseudospectral algorithm to simulate rotating flows in cylindrical cavities

Noele Peres, Sébastien Poncet, Eric Serre

A 3D pseudospectral algorithm to simulate rotating flows in cylindrical cavities

N. Peres, S. Poncet and E. Serre

Abstract When simulating flows in cylindrical rotating cavities a difficulty arises from the singularities appearing on the axis. Its singularities are due to the presence of terms $1/r^n$ ($n = 1,2$) in the Navier-Stokes equations, where r is the radial distance. To avoid evaluating differential equation coefficients which are infinite at that point, the grid must exclude the origin or specific pole conditions must be imposed. An efficient and accurate pseudo-spectral method has been here developed using collocation Chebyshev polynomials in the radial and axial directions and Fourier approximation in the azimuthal direction. To avoid the difficulty on the axis without prescribing any pole conditions, a new approach based on the work of Heinrichs [W. Heinrichs J. Comp. Phys. 199 (2004) 66-86] has been developed. The calculation domain is defined as $(r,\theta,z) \in [-1,1] \times [0,2\pi] \times [-1,1]$ using an even number N of collocation points in the radial direction. Thus, $r = 0$ is not a collocation point. The clustering of collocation points around the rotation axis is also avoided due to the utilization of a Gauss-Lobatto distribution. The flow being indeed laminar close to the axis in most of the rotating flows. In the azimuthal direction, the overlap in the discretization is avoided by introducing a shift equal to $\pi/2K$ (K the number of mesh points in θ-direction) for $\theta > \pi$ in the Fourier transform. The accuracy of the method was checked on the exact steady and unsteady analytical solutions and the capability of the method to simulate complex flows is illustrated considering the well documented case of the vortex breakdown phenomenon.

N. Peres · S. Poncet · E. Serre
Laboratoire de Mécanique, Modélisation et Procédés Propres (M2P2), IMT La Jetée, Technopôle de Château Gombert, 38 rue F. Joliot Curie, 13451 Marseille, France, e-mail: noele.peres@l3m.univ-mrs.fr

1 Introduction

The use of a cylindrical coordinate system introduces a numerical difficulty due to the so-called cylindrical coordinate singularity. Some studies have considered the special behaviour of flow equations at the origin of cylindrical coordinate systems and have proposed different techniques. Apparently, these approaches depend greatly on whether the spectral, finite-volume or finite-difference method is used but in fact there are some similarities between them.

The singularity is due to the presence of terms $1/r^n$ $(n = 1,2)$ in the Navier-Stokes equations governing the flow (r the radial distance), although the flow field itself does not exhibit any singular behaviour on the axis. The treatment of the cylindrical coordinate singularity can be done adequately by means of several techniques taking into account the spatial discretization method and the flow characteristics.

In the context of spectral methods, Boyd and Yu [1] listed several options of radial basis sets and radial grids for a finite cylindrical domain. These methods developed with the objective of capturing the solution near the coordinate singularity include methods that expand the solution in specially designed basis functions, such as spherical harmonics, parity-modified Fourier series, modified Robert functions and eigenfunctions of singular Sturm-Liouville problems among others.

Heinrichs [2] proposed spectral collocation schemes to solve the Poisson problem on the unit disc by discretizing the equations over the whole diameter and choosing an even number of collocation points in that direction. This method has been here extended to solve the full Navier-Stokes equations. An angular shift is introduced in the Fourier transform that avoid pole and parity conditions usually required. It presents some advantages, among others: it keeps the spectral convergence that reduces the number of grid points with respect to lower-order numerical methods. The grid-points distribution densifies the mesh only near the boundaries that makes the algorithm well-suited to simulate rotating cavity flows where thin layers develop along the walls. The reader can refer to Bernardi et *al*. [3] for a complete overview of the different methods treating this singularity using spectral methods.

2 Mathematical modelling and numerical approximation

Cylindrical cavities of radius R and height H will be considered in the following. The motion of an incompressible fluid within such a cavity is governed by the 3D Navier-Stokes equations written in the velocity-pressure formulation and the continuity equation. The components of the velocity vector $\mathbf{V}$ are denoted u, v and w in the cylindrical coordinate system (r,θ,z) and P is the pressure. The momentum and continuity equations, in dimensionless form, can be written in the domain D of border ∂D as:

$$\frac{\partial \mathbf{V}}{\partial t} + (\mathbf{V}.\nabla)\mathbf{V} = -\nabla P + \frac{1}{Re}\Delta \mathbf{V} + \mathbf{F} \text{ in D}, \quad \nabla.\mathbf{V} = 0 \text{ in D} \tag{1}$$

where t is the time and $\mathbf{F}$ represents a given body force. Appropriate boundary conditions of Dirichlet type for the velocity vector can be written as $\mathbf{V} = \mathbf{W}$ on ∂D, with Δ the vectorial Laplacian operator.

The resolution of Equations (1) together with appropriate boundary conditions leads to a Stokes problem coupling velocity and pressure. The collocation method requires boundary conditions in the physical space that can lead to an indetermination at $r = 0$ when the domain is discretized over the radius for $r \in [0, R]$ as in [4]. Here, the computational domain is discretized in the radial direction over the whole diameter between $-R$ and R with an even number N of Gauss-Lobatto collocation points, $r_i = cos(i\pi/N)$, $0 \leq i \leq N$. Thus, no collocation point is located at $r = 0$ and no pole conditions are required.

For a given even number of points K, a shift equal to $\pi/(2K)$ for $\theta > \pi$ is introduced in the angular discretization over $[0, 2\pi]$, as formerly proposed by Heinrichs [2] to solve two-dimensional Poisson equations on an unit disc. According to the angular shift, the following discrete angles θ_j are defined by:

$$\theta_j = \begin{cases} (j-1)\frac{2\pi}{K} & \text{if} \quad j = 1, ..., \frac{K}{2}, \\ \pi + \frac{\pi}{K} + \left(j - \left(\frac{K}{2}+1\right)\right)\frac{2\pi}{K} & \text{if} \quad j = \frac{K}{2}+1, ..., K. \end{cases} \tag{2}$$

Figure 1(a) represents an example for $K = 8$. Such discretization clearly leads to a better resolution in the azimuthal direction with twice the amount of points although the number of Fourier modes remains equal to $K/2$. An example of the 3D grid is shown on Figure 1(b). The distribution of Gauss-Lobatto collocation points over the diameter tightens the points within the boundary layers along the walls and avoids unnecessary clustering of points around the axis.

According to this angular discretization, the following real Fourier basis can be introduced:

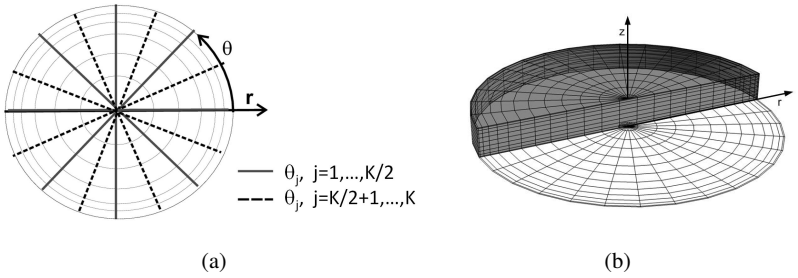

(a) (b)

Fig. 1 Grid structure: (a) Discrete angle θ_j distribution defined by Equation (2) in a (θ, z) plane showing the angular shift. Black and dashed diameters correspond to discretization indices $j = 1, ..., \frac{K}{2}$ and $j = \frac{K}{2}+1, ..., K$, respectively. Grey circles show the radial mesh distribution; (b) Example of 3D mesh discretization in a thin interdisc cavity.

$$\Phi_k(\theta) = \begin{cases} \sin(\mathrm{k}\theta) & \text{if} \quad k = 1,...,\frac{K}{2}-1, \\ \cos(\mathrm{k}\theta) + \sin(\mathrm{k}\theta) & \text{if} \quad k = \frac{K}{2}, \\ \cos\left(\left(\mathrm{k} - \left(\frac{\mathrm{K}}{2}+1\right)\right)\theta\right) & \text{if} \quad k = \frac{K}{2}+1,...,K. \end{cases} \tag{3}$$

that corresponds to the $K \times K$ transformation matrix in the spectral space $P_\theta = (\Phi_k(\theta_j))$, with $j,k = 1,...,K$. According to this basis, the first derivation of any variable is given by the matrix product $D_\theta P_\theta^{-1}\Psi$, where D_θ is the $K \times K$ full matrix $D_\theta = \left(\Phi_k'(\theta_j)\right)_{1\le j,k\le K}$. For $1 \le j \le K$. $\Phi_k'(\theta_j)$ can be written as:

$$\Phi_k'(\theta_j) = \begin{cases} k\cos\left(\mathrm{k}\theta_\mathrm{j}\right), & \mathrm{k} = 1,...,\frac{\mathrm{K}}{2}-1, \\ -k\sin\left(\mathrm{k}\theta_\mathrm{j}\right) + \mathrm{k}\cos\left(\mathrm{k}\theta_\mathrm{j}\right), & \mathrm{k} = \frac{\mathrm{K}}{2}, \\ -\left(k - \left(\frac{K}{2}+1\right)\right)\sin\left(\left(\mathrm{k} - \left(\frac{\mathrm{K}}{2}+1\right)\right)\theta_\mathrm{j}\right), & \mathrm{k} = \frac{\mathrm{K}}{2}+1,...,\mathrm{K}. \end{cases}$$

As referred by Peyret [5], numerical calculations have shown that the presence of the term at $k = K/2$ may lead to instabilities in time-dependent problems mainly because the first derivative cannot be represented in this basis. Therefore the mode $K/2$ must be filtered. The second-order derivative in Fourier space can be written as:

$$\hat{D}_\theta^2 = \begin{cases} -\mathrm{diag}\left(\mathrm{k}^2\right) & \text{if} \quad k = 1,...,\frac{K}{2}, \\ -\mathrm{diag}\left(\left(\mathrm{k} - \left(\frac{\mathrm{K}}{2}+1\right)\right)^2\right) & \text{if} \quad k = \frac{K}{2}+1,...,K. \end{cases} \tag{4}$$

Fast Fourier Transform algorithm (FFT) based on Equation (3) is not yet available. Consequently, the Fourier transform in the azimuthal direction is performed here by matrix products using the subroutine *DGEMM* of the Blas (Basic Linear Algebra Subprograms) library.

The velocity-pressure coupling is solved using the 3D projection algorithm proposed by Raspo et *al*. [6]. It is an improved version of the Goda's algorithm, which introduces a preliminary step for the pressure in order to allow a temporal evolution of the normal pressure gradient at the boundaries. It is based on a semi-implicit second-order scheme that combines an implicit backward Euler scheme for the diffusive terms and an explicit Adams-Bashforth extrapolation for the convective nonlinear terms.

All variables Ψ are spatially discretized using a collocation-Chebyshev method for both non-homogeneous directions (r,z) and a Fourier-Garlekin approximation in the azimuthal direction θ. Numerical solution is thus sought under the form of the following truncated series:

$$\Psi_{NKM}(\bar{r},\theta,\bar{z}) = \sum_{k=1}^{K}\sum_{n=0}^{N}\sum_{m=0}^{M}\hat{\Psi}_{nkm}T_n(\bar{r})\,T_m(\bar{z})\,\Phi_k(\theta) \tag{5}$$

where T_n and T_m are Chebyshev polynomials of highest degrees N and M respectively. $(\bar{r},\bar{z})$ denote the dimensionless space variables (r,z) mapped into the square $[-1,1]\times[-1,1]$, a requisite for the use of Chebyshev polynomials. N and M correspond to the number of Gauss-Lobatto collocation points defined as the extrema of the Chebyshev polynomials of highest degrees N and M. $\Phi_k(\theta)$ are the trigonometric basis functions defined in Equation (3) and K defines the cut-off frequency of the Fourier series that corresponds to $K/2$ modes. The explicit non-linear terms are calculated using the pseudospectral techniques described in [5], where the derivatives in each space direction are calculated in the spectral space and the products are performed in the physical one. The derivatives of implicit diffusion terms are all performed in the physical space using matrix products.

The coupling between the first two components of the vectorial cylindrical Laplacian usually requires a splitting of the operator in an implicit and an explicit part that leads to time-step limitations. Therefore, the variable transformation $u_+ = u + iv$ and $u_- = u - iv$ ($i^2 = -1$) is introduced [7], that makes the Laplacian diagonal:

$$(\Delta V)_+ = \left(\nabla^2 - \frac{1}{r^2} + \frac{2i}{r^2}\frac{\partial}{\partial\theta}\right) u_+ \tag{6}$$

$$(\Delta V)_- = \left(\nabla^2 - \frac{1}{r^2} - \frac{2i}{r^2}\frac{\partial}{\partial\theta}\right) u_- \tag{7}$$

$$(\Delta V)_z = \nabla^2 w \tag{8}$$

Such transformation requires the reorganization in the complex plane of the Fourier coefficients matrix $\widehat{\Psi}$ as follows:

$$\widehat{\Psi} = \begin{cases} \left(\widehat{\Psi}_{j,\frac{K}{2}+k}\right) & , \ k=1, \\ \left(\widehat{\Psi}_{j,\frac{K}{2}+k} + i\widehat{\Psi}_{j,k-1}\right) & , \ k=2,...,K/2 \end{cases} \tag{9}$$

for $1 \le j \le N \times M$. The Fourier mode $K/2$ has been set to zero [5] as previously mentioned. In accordance with the variable transformation previously referred, the spectral matrices $\widehat{u}_+$ and $\widehat{u}_-$ can be written as: $\widehat{u}_+ = \widehat{u} + i\widehat{v}$ and $\widehat{u}_- = \widehat{u} - i\widehat{v}$. Thus,

$$\widehat{u}_+ = \begin{cases} \left(\widehat{u}_{j,\frac{K}{2}+k} + i\widehat{v}_{j,\frac{K}{2}+k}\right) & , \ k=1, \\ \left(\widehat{u}_{j,\frac{K}{2}+k} - \widehat{v}_{j,k-1}\right) + i\left(\widehat{u}_{j,k-1} + \widehat{v}_{j,\frac{K}{2}+k}\right) & , \ k=2,...,K/2 \end{cases} \tag{10}$$

$$\widehat{u}_- = \begin{cases} \left(\widehat{u}_{j,\frac{K}{2}+k} + i\widehat{v}_{j,\frac{K}{2}+k}\right) & , \ k=1, \\ \left(\widehat{u}_{j,\frac{K}{2}+k} + \widehat{v}_{j,k-1}\right) + i\left(\widehat{u}_{j,k-1} - \widehat{v}_{j,\frac{K}{2}+k}\right) & , \ k=2,...,K/2 \end{cases} \tag{11}$$

Finally, the coefficients $\widehat{u}_{j,\frac{K}{2}+k}$, $\widehat{u}_{j,k-1}$, $\widehat{v}_{j,\frac{K}{2}+k}$ and $\widehat{v}_{j,k-1}$ write for $1 \leq k \leq K/2$:

$$\begin{cases} \widehat{u}_{j,\frac{K}{2}+k} = Re\left(\frac{\widehat{u}_+ + \widehat{u}_-}{2}\right), & \widehat{u}_{j,k-1} = Im\left(\frac{\widehat{u}_+ + \widehat{u}_-}{2}\right) \\ \widehat{v}_{j,\frac{K}{2}+k} = Im\left(\frac{\widehat{u}_+ - \widehat{u}_-}{2}\right), & \widehat{v}_{j,k-1} = Re\left(\frac{\widehat{u}_- - \widehat{u}_+}{2}\right) \end{cases} \tag{12}$$

The time-discretization and the Fourier-Galerkin approximation described above lead to a set of elliptic equations for each Fourier wave to be solved in a 2D domain depending on the two non-periodic directions (r,z). Successive 2D Helmholtz and Poisson equations can be written in the matrix form as:

$$A\Psi + \Psi B^T = S \tag{13}$$

with $A = D_r^{(2)} - \frac{1}{r}D_r^{(1)} - \sigma^{(\Psi)}I$ and $B = \left(D_z^{(2)}\right)$. It is noted that only B does not depend on the harmonic k. The Dirichlet boundary conditions are taken into account in S, while the Neumann boundary conditions appear in A or B according to the direction. These 2D algebraic linear systems are solved directly using a full diagonalization technique for each Fourier mode [6].

3 Accuracy and validation of the method

The method is validated for flows in shrouded cylindrical rotor-stator cavities of aspect ratio $G = 2R/H$ (R the disc radius and H the interdisc spacing). The fluid of kinematic viscosity ν is driven by the rotation of the top disc at constant speed Ω, the other walls being at rest. The characteristics scales for space, time and velocity are H, Ω^{-1} and ΩR respectively. The main flow is governed also by the rotational Reynolds number defined as $Re = \Omega R^2/\nu$. The accuracy of the method is checked by using the steady and unsteady divergence-free velocity field $\mathbf{V_e} = (u_e, v_e, w_e)$ for a cavity of aspect ratio $G = 10$ and at a Reynolds number $Re = 250$. The velocity field $\mathbf{V_e}$ satisfies homogeneous Dirichlet boundary conditions. The space and time accuracy is evaluated by computing the discrete error at the inner collocation points, fully described in Raspo et *al*. [6].

For the exact steady solution, the computations are initialized using the disturbed velocity field $\mathbf{V}_0 = \mathbf{V}_e + 1/(200\pi^2) * \mathbf{V}_e$. The time step is fixed at $\delta t = 5 \times 10^{-3}$. The steady solution is assumed to be obtained when the residuals $Res(\Psi) = max_{i,k,j}|\Psi^n_{NKM}(r_i,\theta_k,z_j) - \Psi^{n-1}_{NKM}(r_i,\theta_k,z_j)|/\delta t$ are below 10^{-10}. The spectral convergence of the method is obtained for all variables. The error reported in Figure 2(a), decays exponentially to the zero machine for $N = M = K = 28$ then slightly increases due to the round-off error as usually observed [6].

The exact time-dependent solution is time periodic with a period $T = 0.125$ and the computations are initialized with $V_0 = V_e(t = 0)$. The mesh is fixed at

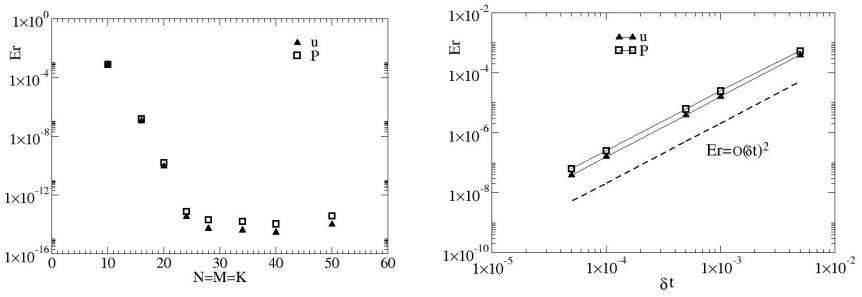

(a) (b)

Fig. 2 Space and time accuracy of the method for exact solutions. Evolution of the error at the inner collocation points Er for the radial velocity component u and for the pressure P: (a) versus the polynomial degrees $N = M = K$, (b) versus the time step δt.

$N = M = K = 40$ and the time step is decreased from $\delta t = 5 \times 10^{-3}$ to 5×10^{-5}. Neumann boundary conditions are used for the pressure. When the periodic state is reached, the time accuracy is evaluated by computing the maximum of $Er(t)$ for $\Psi = (u, v, w, P)$ over the computational time. The results show for all variables that the method is second-order accurate. The maximum of the error $Er(t)$ is reported for the radial velocity component u and for the pressure P in Figure 2(b).

4 Results

The capability of the method to simulate complex flows is illustrated considering the well documented case of the vortex breakdown phenomenon, which may appear in small aspect ratio cavities depending on the Reynolds number. Such flow produces physical phenomena of weak intensity with respect to the base flow in the vicinity of the axis, that still today challenge all numerical solvers. Velocity boundary conditions are no-slip on all walls and $v = \bar{r}$ at the rotating disc. The singularity at the junction between the stationary cylinder and the rotor is appropriately regularized by using an exponential smoothing of the v-profile as proposed in [4].

The confined vortex flow can undergo breakdown for certain combinations of (G, Re). The vortex breakdown phenomenon occurs as an abrupt change in the structure of the vortex core around the cylinder axis and typically develops downstream into a stagnation zone in the flow. Escudier [8] showed experimentally that several recirculation bubbles may exist on the main vortex axis. The accuracy of the algorithm to simulate secondary vortices around $r = 0$ is shown on simulations covering the 3D vortex breakdown. The mesh size is fixed at $126 \times 48 \times 65$ in the radial, azimuthal and axial directions respectively and the time step is equal to 10^{-2}.

At $Re = 6500$, the flow is fully three-dimensional with some asymmetries in the breakdown structure (Fig. 3). The vortex breakdown is related here to the 'S-shaped' regime first noted by Escudier [8]. The solution is similar to the one obtained by DNS [9] and characterized by a precessing structure around the axis in the direction of the main flow. At this Reynolds number, the temporal regime is chaotic due to the interaction of boundary layer instability patterns with the precessing bubble.

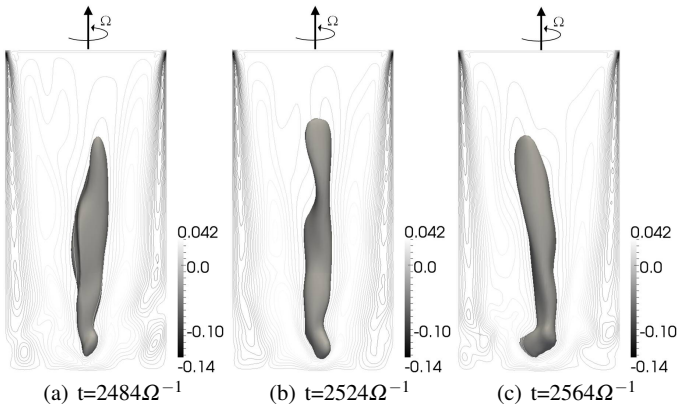

Fig. 3 Unsteady and three-dimensional 'S-shaped' vortex breakdown for $(G = 0.5, Re = 6500)$. Snapshots of $w = 0$ isosurface and isolines of the axial velocity component w at different times.

The precession motion of the structure is still not fully understood and it is possibly related to a symmetry breaking of the structure with respect to the $m = 1$ mode as suggested by Marques and Lopez [10]. Some simulations have been here performed at $Re = 5500$ together with a nonlinear normal form analysis based on linear global modes by P. Meliga (private communication). Figure 4 presents the kinetic energy of the mode $m = 1$ for several Reynolds number Re, showing the consistence of the results with the theoretical analysis of P. Meliga (private communication).

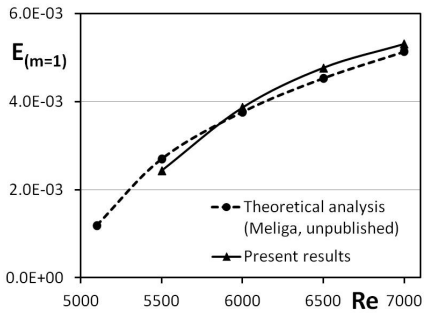

Fig. 4 Kinetic energy of the mode $m = 1$, $E_{(m=1)}$, versus the Reynolds number Re for $G = 0.5$.

Snapshots of $w = 0$ isosurface and isocontours of w show on Figure 5 the full and filtered solutions. In agreement with the theoretical analysis of Meliga, the results show that 3D modes of centrifugal instability within the vertical boundary layers are related to azimuthal wave numbers strictly larger than one since by keeping the modes $m = 0$ and $m = 1$ only, the main flow becomes almost axisymmetric (Fig.5(a)-5(c)). In contrast, the vortex breakdown topology does not change and the precession seems related to a $m = 1$ mode of instability as confirmed by the new filtered solution on Figures 5(g)-5(i). Moreover, transition of the solution to the $m = 1$ mode as well as its amplitude match well with the theoretical predictions.

5 Conclusions

A spectrally convergent method has been proposed to solve the three-dimensional Navier-Stokes equations in cylindrical coordinates without any requirement of polar or parity condition, as in most of the methods proposed in the literature. To perform that, the equations have been discretized over the whole cavity diameter using a Gauss-Lobatto collocation point distribution that avoids any clustering of points in the stable region around the axis. In addition, an angular shift has been introduced in the azimuthal discretization that allows a more efficient discretization of the physical space in this direction. Numerical solutions for the vortex breakdown phenomenon match previous results available in the literature.

References

1. J. P. Boyd and F. Yu. Comparing seven spectral methods for interpolation and for solving the Poisson equation in a disk: Zernike polynomials, Logan-Shepp ridge polynomials, Chebyshev-Fourier series, cylindrical Robert functions, Bessel-Fourier expansions, square-to-disk conformal mapping and radial basis functions. *J. Comput. Phys.*, 230:1408–1438, 2011.
2. W. Heinrichs. Spectral collocation schemes on the unit disc. *J. Comp. Phys.*, 199:66–86, 2004.
3. C. Bernardi, M. Dauge, and Y. Maday. *Spectral Methods for Axisymmetric Domains*. Ser. Appl. Math. 3, 1999.
4. E. Serre and J.P. Pulicani. A three-dimensional pseudospectral method for rotating flows in a cylinder. *Comput. Fluids*, 30:491–519, 2001.
5. R. Peyret. *Spectral methods for incompressible viscous flow*. Springer-Verlag, 2002.
6. I. Raspo, S. Hugues, E. Serre, A. Randriamampianina, and P. Bontoux. A spectral projection method for the simulation of complex three-dimensional rotating flows. *Comput. Fluids*, 31:745–767, 2002.
7. S.A. Orszag and A.T. Patera. Secondary instability of wall-bounded shear flows. *J. Fluid Mech.*, 128:347–385, 1983.
8. M. P. Escudier. Observations of the flow produced in a cylindrical container by a rotating end wall. *Exp. Fluids*, 2:176–186, 1984.
9. E. Serre and P. Bontoux. Three-dimensional swirling flow with a precessing vortex breakdown in a rotor-stator cylinder. *Phys. Fluids*, 13:3500–3503, 2001.
10. F. Marques and J. M. Lopez. Precessing vortex breakdown mode in an enclosed cylinder flow. *Phys. Fluids*, 13:1679–1682, 2001.

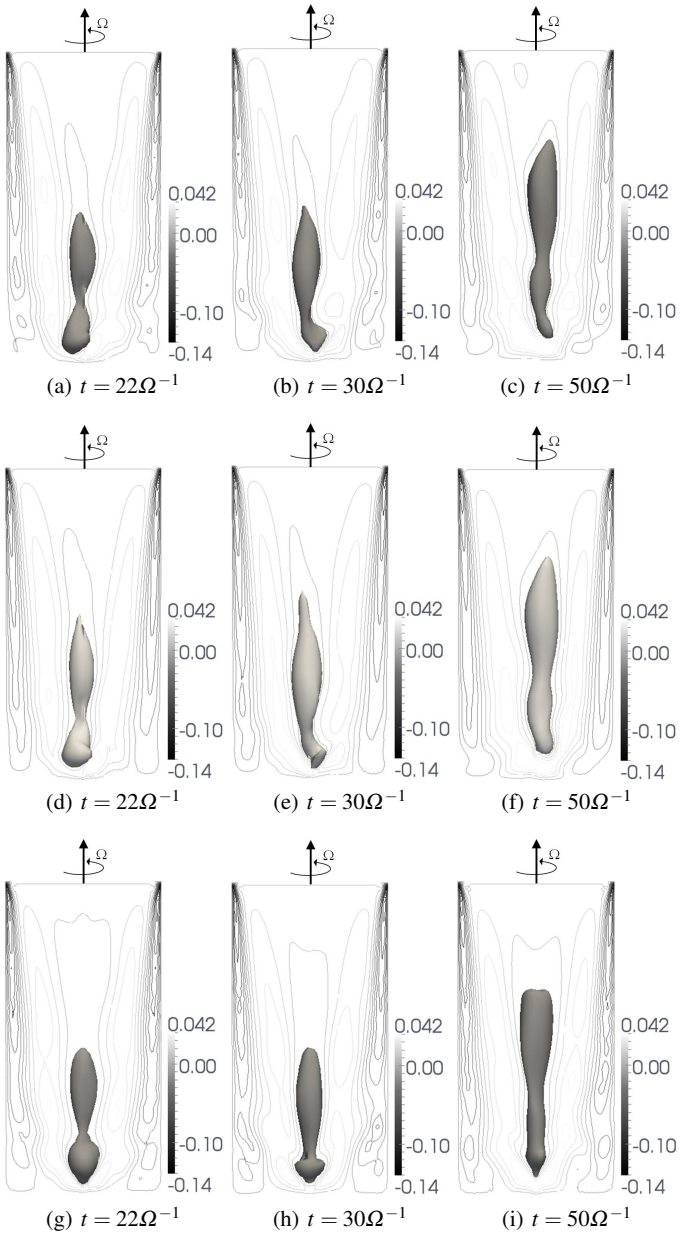

(a) $t = 22\Omega^{-1}$ (b) $t = 30\Omega^{-1}$ (c) $t = 50\Omega^{-1}$

(d) $t = 22\Omega^{-1}$ (e) $t = 30\Omega^{-1}$ (f) $t = 50\Omega^{-1}$

(g) $t = 22\Omega^{-1}$ (h) $t = 30\Omega^{-1}$ (i) $t = 50\Omega^{-1}$

Fig. 5 Role of the $m = 1$ mode in the precession. Snapshots of $w = 0$ isosurface and isocontours of w in a (r,z) plane for $(G = 0.5, Re = 5500)$ at different times $t = 22\Omega^{-1}$, $t = 30\Omega^{-1}$ and $t = 50\Omega^{-1}$. (a,b,c) full solution, (d,e,f) filtered solution for all modes $m > 1$ and (g,h,i) solution where only the mode $m = 1$ is filtered.